ISSN 0016-7029, Geochemistry International, 2017, Vol. 55, No. 4, pp. 317–329. © Pleiades Publishing, Ltd., 2017.
Original Russian Text © N.R. Khisina, S.N. Teplyakova, R. Wirth, V.G. Senin, A.A. Averin, A.A. Shiryaev, 2017, published in Geokhimiya, 2017, No. 4, pp. 287–301.

Carbon-Bearing Phases in Shock-Induced Melt Zones of the Elga Meteorite

N. R. Khisina[a], *, S. N. Teplyakova[a], R. Wirth[b], V. G. Senin[a], A. A. Averin[c], and A. A. Shiryaev[c]

[a]*Vernadsky Institute of Geochemistry and Analytical Chemistry (GEOKhI), Russian Academy of Sciences, Moscow, 119991 Russia*

[b]*Helmholtz-Zentrum Potsdam, Deutsches GeoForschungsZentrum—GFZ, Telegraphenberg B-14473 Potsdam, Germany*

[c]*Frumkin Institute of Physical Chemistry and Electrochemistry, Russian Academy of Sciences, Moscow, 119071 Russia*

**e-mail: khisina@geokhi.ru*

Received May 19, 2016; in final form, June 28, 2016

Abstract—The mineralogy and texture of shock-induced melt veinlets and melt pockets in silicate inclusions in the Elga IIE iron meteorite have been studied by reflected-light optical microscopy, EMPA, SEM, Raman spectroscopy and TEM. The results suggest that Elga experienced two discrete impact events. The earlier event involved the collision of a metallic projectile with a silicate target and resulted in partial melting and recrystallization of the silicate material, forming schreibersite and oxide rims between the metal and silicate. The later impact event resulted in melt pockets in the silicate inclusions and was associated with fragmentation, melting, and brecciation of the rims and displacement of some fragments into the melt pockets. These fragments are shown to contain carbon-bearing phases: siderite and amorphous sp^2 carbon, which form carbon–oxide, siderite–oxide, and siderite–schreibersite associations. The fact that the carbon-bearing fragments are spatially constrained to shock breccia and melt zones indicates that these fragments are genetically related to the impact process and that their carbon-bearing phases are of cosmic origin.

Keywords: Elga meteorite, melt pockets, brecciation, shock metamorphism, siderite in an IIE iron meteorite, amorphous carbon in an iron IIE meteorite, TEM, Raman spectroscopy

DOI: 10.1134/S0016702917040036

INTRODUCTION

Iron meteorites are Fe–Ni alloys with dominant phases of kamacite (α-(FE,Ni), 5–7% Ni), taenite (γ-(FE,Ni), 20–25% Ni), and plessite (fine-grained mixture of kamacite and taenite). Fraction of the accessory minerals does not exceed 10% of these minerals. They are represented by phosphide (schreibersite (Fe,Ni)P), carbide (Fe_3C), and sulfides (troilite FeS). The metal sometimes also hosts oxygen-bearing phases: chromite $FeCr_2O_4$ and single crystals of phosphates, silicates, and stishovite. Among the currently known 1125 iron meteorites, a group of meteorites is distinguished that contain silicate inclusions in the metal. The inclusions range from a few fractions of a millimeter to a few centimeters across and consist of polymineralic granular aggregates or incompletely recrystallized silicate glass. Among all iron meteorites only 45 host silicate inclusions. According to the systematics currently adopted in meteoritics and based on chemical and petrological characteristics of the silicate material (Ulff-Møller et al., 1995), most iron meteorites with silicate inclusions make up chemical group IAB (33 meteorites), eight meteorites are ascribed to group IIE, and four compose group IVA. Silicate inclusions in IAB meteorites are metal–chondrite breccia (Ulff-Møller et al., 1995). Silicate inclusions in IIE meteorites are the most diverse in texture and in chemical and mineralogical composition and vary from primitive, which retain the chondritic texture and composition, to inclusions whose composition is more similar to that of terrestrial alkaline rhyolite. The enrichment of inclusions of the rhyolite type in Na_2O, K_2O, and SiO_2 to levels typical of terrestrial alkaline rhyolite is difficult to explain by either partial melting or fractional crystallization of chondritic material. At the same time, genetic relations with primitive (chondritic) material follow from similarity of the oxygen isotopic composition of these inclusions to that in ordinary chondrites of group H (Clayton et al., 1983).

A number of hypotheses were suggested to explain the occurrence of silicate inclusions in the metal of iron meteorites. The paradigm is the hypothesis of impact melting and mixing in the parent body of H chondrite composition as a result of a collision with a metallic projectile (Olsen et al., 1994; Casanova et al., 1995; Ikeda and Prinz, 1996; Gaffey and Gilbert, 1998; McDermott et al., 2014). Alternative hypotheses are the formation at the core–mantle boundary and subsequent impact heating (McCoy,

1995) and the "condensation" hypothesis (Kurat et al., 2005, 2007), according to which the silicate inclusions were formed in the nebula by condensing liquid.

The mineralogical, chemical, and textural diversity of the silicate inclusions in IIE meteorites complicates assignment of the IIE silicates to a single parent body of IIE meteorites. Moreover, the variations were detected even between discrete inclusions in a single meteorite: for example, the Elga meteorite was determined to contain inclusions of five petrologic types (Osadchii et al., 1981). In several instances, the silicate material of IIE meteorites shows evidence of unequilibrated crystallization. The silicate minerals are highly unequilibrated with the glass in silicate inclusions in IIE meteorites (Kurat et al., 2007), and this fact cannot be explained by the fractional crystallization of a single initial composition. The extremal enrichment of the silicate inclusions of the Elga meteorite in Si, K, Na, Rb, and Nb and the occurrence of negative Eu anomalies may suggest that the inclusions were formed by partial melting of a source that had previously underwent plagioclase fractionation (Teplyakova et al., 2010). Several IIE iron meteorites show evidence of an impact event and host so-called melt pockets, which are domains of silicate material or metal affected by impact melting (Osadchii, 1981; Teplyakova, 2011).

We have studied mineralogy and texture of the shock-induced melt veins and melt pockets in silicate inclusions in the Elga IIE iron meteorite by reflected-light optical microscopy, EMPA, SEM, Raman spectroscopy, and TEM. The results suggest that the evolutionary history of Elga involved two discrete impact events. The older one resulted from the collision of a metallic projectile with silicate target and induced the partial melting and recrystallization of the material, accompanied by formation of schreibersite and oxide rims at interfaces between the metal and silicate. The younger impact event produced melt pockets in the silicate inclusions and was associated with the shattering, melting, and brecciation of these rims and displacement of some of their fragments into the melt pockets. These fragments host carbon-bearing phases: siderite and amorphous sp^2 carbon, which form carbon–oxide, siderite–oxide, and siderite–schreibersite associations. The spatial association of the fragments to the impact brecciation and melt zones suggests that they were genetically related to the impact process and that the carbon-bearing phases are of cosmic genesis.

FIND OF THE ELGA METEORITE AND ITS BRIEF CHARACTERIZATION

The Elga meteorite was found on August 28, 1959, at the Razvedchik gold field in the basin of the Elga River, a large left-hand tributary of the Indigirka in its upper reaches, in the territory of Yakutia. The meteorite was found when gold-bearing sand was washed, with the sand recovered from a production mine in the valley of Promezhutochnyi Stream, a right-hand tributary of the Elga. The meteorite was found in pebble material lifted from a depth of 20 m. Promezhutochnyi Stream is a relatively small watercourse, in a 150–200 m wide valley and no more than 3 km long. The thickness of the silt in the shaft area is 18 m, it overlays 2–3 m thick layer of alluvial pebbles laying on a bedrock. Analysis of the local geology suggests (Vronskii, 1962) that Elga meteorite fell several thousand years ago on the alluvium of Promezhutochnyi Stream and was then gradually buried beneath the accumulated colluvium.

The area is characterized by widespread permafrost, so that the gold-bearing sands are recovered by underground work with the use of blast. Upon blasting, the rock is lifted to the surface and, upon thawing, turns into loose material. The latter is loaded onto a belt conveyer and brought to sluicing facilities to separate gold. On August 28, 1959, the sluicing box was operated by E.N. Urusov, a geologist at the local geological survey. He notices a large black "boulder" of unusual shape on the belt. Upon close examination of this "boulder", he decided that it was piece of an unusual terrestrial rock.

The meteorite is of irregular, slightly angular morphology, and its natural surface is rounded, uneven, and locally displays a thin platy fabrics and regmaglypt surface topography. The upstanding fine-flow surface areas are of steel-gray color, whereas "depressions" are covered with a black film and, locally, rust-brown material. The mass of the sample is 28.8 kg. A fragment (887.5 g) of the meteorite was transferred to the Meteorite Committee of the USSR Academy of Sciences and was later sawn into several fragments used to prepare thin sections for further analyses.

The Elga meteorite is a fine-grained octahedrite and hosts rounded silicate inclusions a few millimeters across (Plyashkevich, 1962). The texture and composition of the metal and silicate inclusions led Plyashkevich (1962) to conclude that the meteorite shows traces of secondary melting. The bulk composition of the metallic constituent is (D'yakonova et al., 1979) as follows: 90.51 wt % Fe, 8.38 wt % Ni, 0.64 wt % Co, 0.01 wt % Cu, and 0.46 wt % P. Based on its Ni, Ga, and Ge concentrations the meteorite was later assigned to the group IIE (Wasson, 1970). The distribution of trace siderophile elements in the metal of IIE meteorites suggests that these meteorites were produced during the first stages of unequilibrated crystallization of melts from an H chondritic source in a closed system (Teplyakova, 2012). The mineralogy of the meteorite and its features of impact metamorphism are described in detail in (Kvasha, 1974; Osadchii et al., 1981). Silicate inclusions in the Elga meteorite are morphologically and chemically similar to inclusions in the Kodaikanal meteorite and some other iron meteorites of the group IIE, for example, Weekeroo Station and Colomera. The boundaries between the metal and silicate inclusions are lined by

schreibersite rims, which are typical of some IIE meteorites (Ikeda and Prinz, 1996; Kurat et al., 2007). The silicate inclusions in Elga vary broadly in texture, chemistry, and mineralogy. The inclusions were subdivided into five types (Osadchii et al., 1981). This publication also provides a description of the mineralogy of the inclusions and genetic interpretation of the Elga meteorite. According to (Osadchii et al., 1981), the common spread inclusions in Elga are of the following three types. Type I has micropoikilitic structure with clinopyroxene and K–Na feldspar as the dominant minerals and orthopyroxene, phosphates, chromite, and olivine. Type II has microporphyric structure formed by clinopyroxene crystals in glass. Type III consists of fully recrystallized inclusions made up of crystals of clinopyroxene, olivine, and K–Na feldspar. Mössbauer spectroscopy data indicate that clinopyroxene in type-I inclusions has high content of Fe^{3+} (up to 50%) (Osadchii et al., 1981). Petrographic and mineralogical lines of evidence of secondary impact melting of the meteorite are reported in (Plyashkevich, 1962; Osadchii et al., 1981; Teplyakova et al., 2012). Earlier studies of the schreibersite fragments embedded into a silicate melt pocket have identified siderite (Teplyakova et al., 2012).

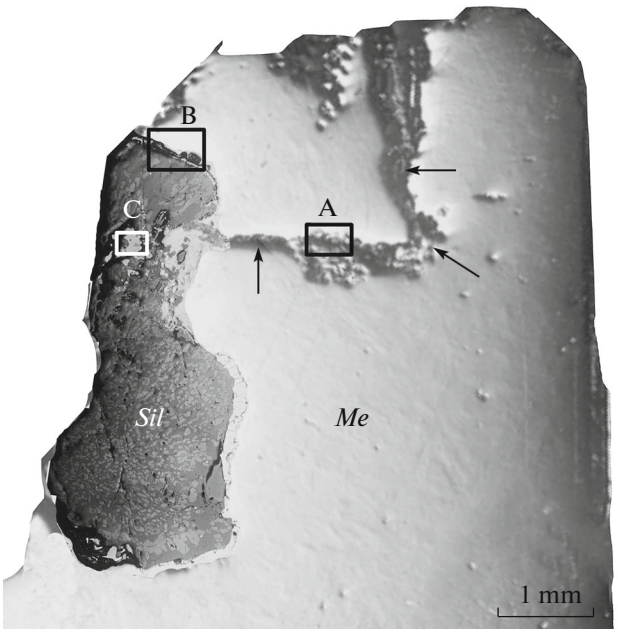

Fig. 1. Part of fragment 2315-3.3 of the Elga meteorite with a silicate inclusion (*Sil*) and a bent silicate vein (indicated by arrows) in metal (white). Rectangles A, B, and C mark areas hosting carbon-bearing phases. Optical micrograph taken in reflected light.

SAMPLES AND METHODS

The mineralogy of the impact transformations in the material was studied in fragments of the Elga meteorite (fragment 2315-3.3; Fig. 1). The fragment 2315-3.3 is approximately 2.2 × 0.9 cm (Fig. 1) and was sawn off a peripheral part of the meteorite. The left-hand boundary of this fragment in Fig. 1 is the surface of the meteorite. The fragment hosts a rounded silicate inclusion of irregular shape, 4.5 × 1.5 mm across, which is connected with a zigzag veinlet cutting across this fragment from its left-hand margin to top (Fig. 1). According to the systematics in (Osadchii et al., 1981), the silicate material of the fragment 2315-3.3 belongs to petrologic type II.

The material was studied under and optical microscope and by EMPA, Raman spectroscopy, and TEM.

Microprobe analyses were carried out on a CAMECA SX 100 (France) at accelerating voltage of 15 kV and beam current of 10 nA. The standards were schreibersite (for Fe, Ni, and P), metallic Co (for Co), andradite (for Si), and diamond (for C). The analyzing crystal for carbon was PC2. Analysis was conducted with a beam defocused to 5 μm. Analysis for carbon was a challenging task. To get rid of the negative charge, the samples for microprobe analysis are conventionally sputter coated with carbon, but this is could not be done in our situation because carbon is one of the elements to be analyzed in the samples. With regard for the small size of the targets to be analyzed and their occurrence in contact with electrically conducting phases (FeNi metal and Fe,Ni phosphide), the analyses were carried out without the coating. The electron images of the sample surface were practically not distorted, which suggests that the charging of the site was insignificant and allowed us to neglect its possible effect on the systematic errors of the analysis. Another serious problem (which cannot be eliminated technically) of the analysis is the need to discriminate between the contaminating carbon (which is produced when the sample is bombarded by the beam) and the element in the sample itself. In view of the aforementioned considerations, the data reported below should be regarded as semiquantitative. Nevertheless, these results led us to certain conclusions concerning the atomic proportions of the Fe, Ni, and C in the analyzed material.

Transmission electron microscopy was performed at the Center of Geological Studies in Potsdam (GeoForschungsZentrum, Potsdam) in Germany and at the Kurchatov Research Center in Moscow, Russia, using Tecnai $G_2$30ST and Titan 80-300 microscopes (Teplyakova et al., 2012; Khisina et al., 2016). Images were acquired in Bright (BF) and Dark (DF) modes; electron energy loss spectroscopy (EELS) was also employed. Chemical analyses were carried out with an energy-dispersive spectrometer (EDS). Chemical mapping and phase-contrast imaging were performed using a high-angle annular dark-field (HAADF) detector. The samples for TEM study were prepared using the method of focused ion beam (FIB) and rectangular foil fragments 10 × 5 μm and 20–100 nm thick. The FIB foils were cut off the thin section to a

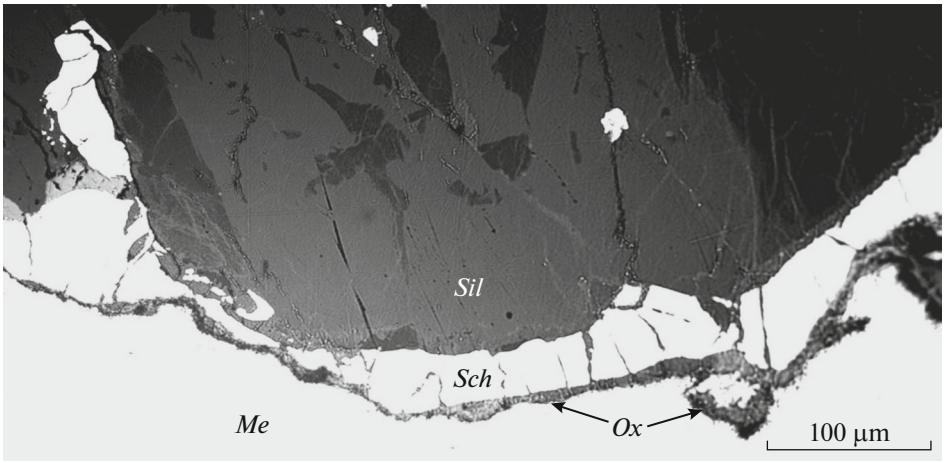

Fig. 2. Schreibersite (white) and oxide (gray) rims at contact of the silicate inclusion (*Sil*) and metal (*Me*). Phases: *Sch*—schreibersite, *Ox*—oxide. Optical micrograph taken in reflected light.

depth of 5 μm perpendicular to its surface, and after thinning were mounted on specialized grits and placed into the holder of the microscope.

The EMPA and TEM studies were conducted with samples not coated with carbon. Prior to each EMPA series, the surface of the samples to be analyzed was repolished and cleaned.

Raman spectra were recorded on a Senterra (Bruker GmbH) spectrometer with a 5 mW laser power, beam 3 μm in diameter on the sample at 532 nm excitation wavelength.

RESULTS

The silicate inclusion itself and the vein connected with it show evidence of shock metamorphism from two discrete impact events experienced the Elga meteorite.

During the older event the collision of a metallic projectile with silicate target lead to partial melting and recrystallization of the material and development of double schreibersite–oxide rims at boundaries between the metal and silicate. A schreibersite rim 50 μm thick was found at the contacts of the silicate inclusion with the metal (Fig. 2). The rim is cut across by numerous transverse cracks and is locally disintegrated. The pure metal and schreibersite rims are separated by a rim of oxidized metal, which is gray in optical (Fig. 2) and BSE images. The composition of the metal near the contact with the oxide rim is $Fe_{0.92}Ni_{0.08}$ (Table 1).

The later impact event produced local pockets of impact melt in the silicate inclusion and, locally, also in the vein (Fig. 3). The melt pockets consist of glass that contains practically no pyroxene crystals, which were dissolved when the impact melt was generated. The glass of the melting pockets has a higher Fe/S ratio than that of the recrystallized glass in nearby regions of the inclusion that did not suffer the impact melting. Traces of impact melting and liquid immiscibility between silicate and phosphide melts in the melt pockets are discernible in the form of submicrometer-sized microglobules hosted in both the silicate glass and the schreibersite fragments and metal–phosphide aggregates moved to the silicate melt (Fig. 3). The microglobules in the silicate melt consist of schreibersite, and those in the metal–schreibersite fragments are of silicate composition. The shock-induced transformations also involved fragmentation of the schreibersite and oxide rims and the adjacent metal with the simultaneous displacement of some of the fragments inward melting pockets in the silicate inclusion (Fig. 3). The impact process typically produced het-

Table 1. Chemical composition (at %) of Ni,Fe-bearing phases in the Elga meteorite (EMPA data)

Setting	Fe	Ni	Co	P	C	Fe/Ni
Metal (meteorite matrix) $Fe_{0.92}Ni_{0.08}$	91.9	7.5	0.6	–	–	11.5
Metal (fragment in a silicate melting pocket) $Fe_{0.93}Ni_{0.07}$	92.6	6.7	0.5	0.2	–	13.8
Schreibersite (globule in silicate glass) $(Fe_{0.8}Ni_{0.2})_3P$	59.7	14.3	0.2	25.8	–	3.9
Schreibersite (rim on a silicate inclusion) $(Fe_{0.8}Ni_{0.2})_3P$	57.6	17.1	0.2	25.1	–	3.4
Metal + schreibersite (fragment in a silicate melting pocket) $Fe_{0.92}Ni_{0.8} + (Fe_{0.77}Ni_{0.23})_3P$	76	11.7	0.4	11.9	–	6.5

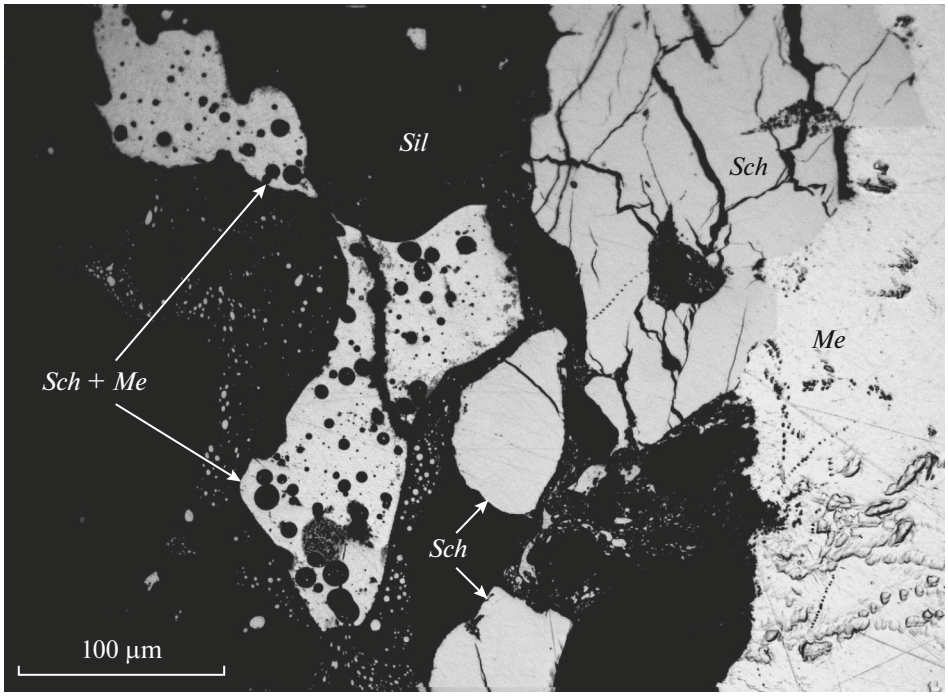

Fig. 3. Melting pocket in the silicate inclusion. The pocket hosts displaced fragments of the brecciated material of the schreibersite rim and metal. The metal–schreibersite fragments host microglobules of silicate glass, and the silicate glass hosts schreibersite microiglobiles. Phases: *Sil*—silicate, *Me*—metal, *Sch*—schreibersite. Optical micrograph taken in reflected light.

erogeneous aggregates of mineral phases at the interface of the metal and silicate material as a consequence of mixing of the impact melts of various chemical composition. For example, chips of mixed metal–phosphide composition (Fig. 3, Table 1) were identified among fragments of the metal and schreibersite rim hosted in the silicate material. The origin of these fragments may be explained by the separation of the schreibersite rim fragments together with the host metal, their embedding into the silicate melt, melting, and subsequent crystallization of the metal–phosphide eutectic. The melting and fragmentation of the material are most obvious at contacts between the metal and silicate in the vein and at the boundaries between the silicate inclusions and metal matrix. The vein is filled with brecciated material of fragments of the silicate glass, metal, schreibersite, and oxide.

The fragmentation and brecciation zones of the rims and in the melt pockets within the silicate material of the meteorite contain unusual carbon-bearing multiphase fragments. Our EMPA, Raman spectroscopic, and TEM studies allowed us to classify the carbon-bearing fragments into three types: siderite–phosphide, siderite–oxide, and graphite–oxide.

CARBON–OXIDE FRAGMENTS

The brecciation zone A (Fig. 1) in the shock-induced vein contains, between the fragments of the schreibersite rim, metal, and silicate material, fragments of the oxide rim with small (<1 μm) dark specks (Figs. 4a, 4b). Microprobe analysis of these specks (the spot analyses inevitably involved the host oxide matrix) show the presence of carbon (Table 2). Raman spectra of domains with the dark specks suggest the occurrence of disordered (amorphous) carbon (with sp^2 hybridized orbitals) in association with Ni-bearing magnetite (magnetite–trevorite solid solution) (Fig. 4c,

Table 2. Cation composition (at %) of carbon-bearing fragments in a impact melting zone in the Elga meteorite (EMPA data)

Type of fragments	Fe	Ni	Co	P	C
A. Carbon–oxide fragment in an oxide rim of the metal C + $(Fe^{2+}_{0.661}Ni_{0.33})Fe^{3+}_2O_4$	76.7	6.5	0.4	0.4	16.0
B. Siderite–oxide fragment in an oxide rim of the metal $FeCO_3 + NiFe_2O_4$	51.5	2.3	0.3	0.6	45.3
C. Siderite–carbon–trevorite–schreibersite fragment in a silicate melting pocket $FeCO_3 + (Fe_{0.79}Ni_{0.21})_3P + NiFe_2O_3$	61.3	18.9	0.3	12.0	7.5

* Analyses are renormalized to analytical totals of 100%

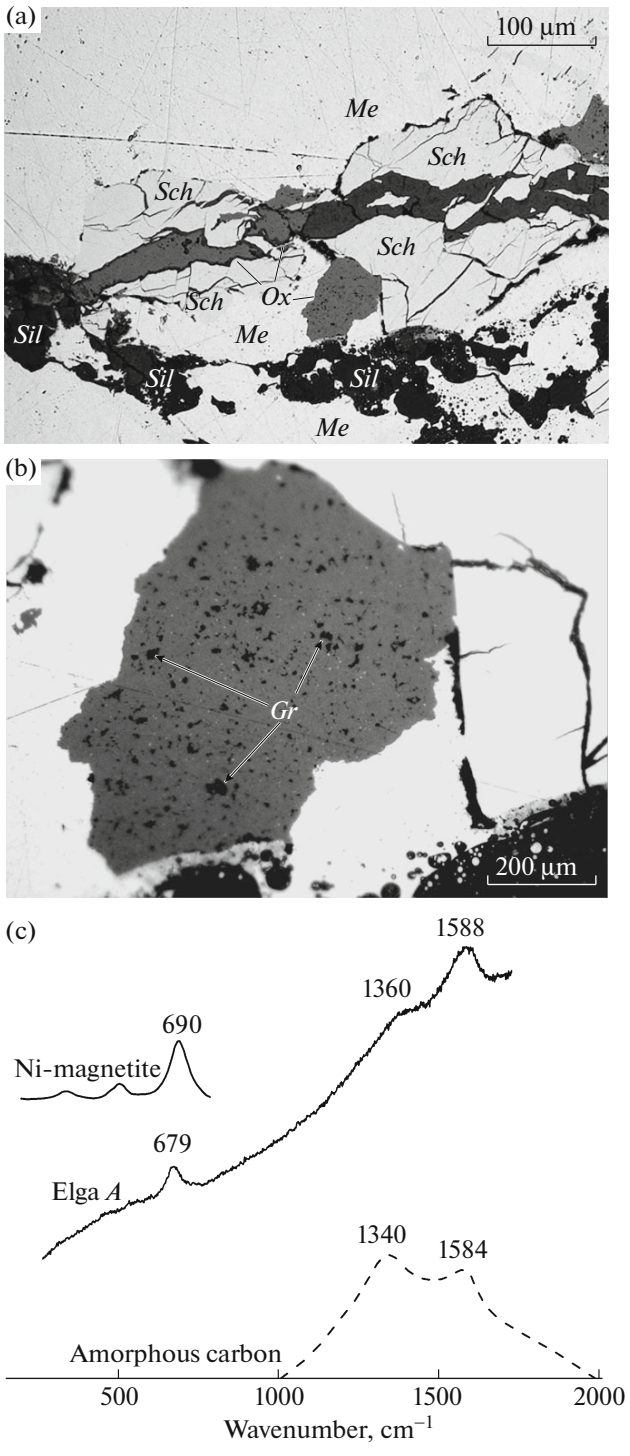

Fig. 4. Amorphous carbon and Ni-magnetite in a brecciation zone in an impact veinlet (Fig. 1, area *A*). (a) Fragments of an oxide rim (gray) with minute dark specks of amorphous carbon among fragments of silicate (*Sil*), metal (*Me*), and schreibersite (*Sch*). Optical micrograph taken in reflected light. (b) Enlarged image of a fragment of the oxide rim with specks of amorphous carbon (*Gr*). (c) Raman spectrum of Elga A, from a part of an oxide fragment with a speck of amorphous sp^2 carbon (see Fig. 4b). The band at 679 cm^{-1} in the Elga A spectrum corresponds to Ni-bearing magnetite with (Fe^{2+}/Ni) >1 : 1, bands at 1340 and 1588 cm^{-1} are ascribed to amorphous carbon. For comparison, the figure shows the Raman spectra of Ni-magnetite (*Ni-Magnetite*) according to (Rana and Johri, 2013) and amorphous carbon (amorphous carbon) in the Murchison carbonaceous chondrite (Larsen and Nielson, 2006).

Table 3). Considering the Raman spectroscopic data, the microprobe analyses (Table 2) were recalculated into a mix of elemental carbon and Ni-bearing magnetite $Fe^{3+}(Fe_{0.66}Ni_{0.33})O_4$ with Fe^{3+}/Ni ratio of 2 : 1. Note that the mode of carbon occurrence is so far uncertain because the Raman spectra of various amorphized or disordered carbon materials with sp^2 hybridized orbitals (macromolecular carbon, amorphous carbon, disordered carbon, etc.) are qualitatively similar. Some conclusions about the phase composition can be derived from data on the dispersion of the D and G peaks, which requires recording spectra at different excitation energies. Unfortunately, the sample contains very little carbon, which made it impossible to record spectrum of reasonably good quality using a 785 nm excitation wave. In view of this the disordered sp^2-carbon phases detected in the Elga meteorite are characterized below using the term *amorphous carbon*, which is utilized in the literature to characterize analogous Raman spectra of carbon in meteoritic material (King et al., 2011; Steele et al., 2012).

SIDERITE–OXIDE FRAGMENTS

Siderite–oxide segregations were found in some portions of the oxidation rim around the metal near the top of the silicate inclusion (area B in Fig. 1). Under an optical microscope and in BSE images, such parts of the oxide rim look patchy (Fig. 5a), with the contrasting domains showing chemical and phase heterogeneity of the segregations. Darker siderite regions in oxide matrix are of irregular shape, are devoid of crystallographic outlines, and have no linear boundaries with the host oxide phase. Microprobe analyses in the dark regions suggest the presence of carbon (Table 2). Raman spectra (Figs. 5b, 5c) recorded in contrasting portions of this fragment led us to believe that the dark-contrast areas correspond to siderite, and the pale-contrast ones are trevorite $NiFe_2O_4$ (Table 3, Fig. 5). It should be mentioned that the main characteristics of lines in the Raman spectra of spinels correspond to vibrations of tetrahedrally coordinated cations. Both pure and Ni-bearing magnetite contains only tetrahedrally coordinated Fe^{3+} ions. Because of this, possible inharmonic contribution of the interaction of octahedrally coordinated ions with Raman-active vibrations is masked by the effects of crystal field excitation by, for example, due to defects. In view of this, the presence of the five major characteristic bands of magnetite spinel in Raman spectra of the

Table 3. Bands (cm^{-1}) in the Raman spectra of carbon-bearing inclusions in the Elga meteorite and identification of carbon-bearing and oxide phases in the inclusions

Carbon–oxide inclusion (Elga)	Siderite–oxide inclusion (Elga)	Siderite–schreibersite inclusion (Elga)	Trevorite (Ahlawat et al., 2011)	Ni-magnetite (Rana and Johri, 2013)	Siderite (Buzgar and Apopei, 2009)	Amorphous carbon (Larsen and Nielsen, 2006)
–	190 (*sid*)	182 (*sid*)	–	–	188	–
–	–	–	–	195	–	–
–	290 (*sid*)	–	–	–	296	–
–	–	–	337	–	–	–
–	–	–	–	324	–	–
470 (Ni-*Mgt*)	–	–	–	472	–	–
–	478 (*trv*)		486	–	–	–
–	–	–	–	–	500	–
552 (Ni-*Mgt*)	–	–	–	559	–	–
	–	–	575		–	–
675 (Ni-*Mgt*)	–	–		679	–	–
–	705 (*trv*)	700 (*trv*)	700	–	–	–
–	734 (*sid*)	735 (*sid*)	–	–	732	–
–	–	–	843	–	–	–
–	1085 (*sid*)	1085 (*sid*)	–	–	1085	–
1360 (*Gr*)	–	1380 (*Gr*)	–	–	–	1342
1588 (*Gr*)	–	1576 (*Gr*)	–	–	–	1584
–	–	–	–	–	–	–

Ni-*Mgt* is Ni-bearing magnetite, *trv* is trevorite, *sid* is siderite, *Gr* is amorphouc carbon.

sample is still insufficient for unambiguous conclusions about the composition (see, for example, Graves et al., 1988). Nevertheless, considered together with the microprobe analyses, these spectra can be interpreted as indicating the presence of trevorite. The microprobe analyses can be reasonably accurately recalculated into mixture of siderite $FeCO_3$ and trevorite $NiFe_2O_4$ (Table 2).

SIDERITE–SCHREIBERSITE FRAGMENTS

A melt pocket in the silicate inclusion contains a group of fragments of irregular patchy morphology, with contrast different from that of the silicate and metal (Fig. 6). Most of these fragments are 20–40 μm in size, and only one of them is as large as 200 μm (Fig. 6). The fragments contain silicate glass globules (Figs. 6, 7). At the magnification of the optical microscope, the fragments are seen to possess unusual "metal graphic" microtextures (Osadchii et al., 1991) defined by ordered distribution of submicrometer dark phases in the schreibersite matrix (Fig. 7a). Microprobe analyses of the mixed composition of the dark-contrast regions and surrounding matrix point to presence of carbon, phosphorus, iron, and nickel (Table 2). The BSE-SEM images (Fig. 7a) show that the sumbicrometer segregations are, in fact, two phases of different contrast: dark gray and pale gray. The Raman spectra of the domains with a dark gray contrast display siderite bands at 182, 735, and 1085 cm^{-1} and weak-intensity bands of amorphous carbon at 1380 and 1576 cm^{-1} (Fig. 7b, Table 3). The Raman spectra of the "pale gray" phase possess a trevorite band at 700 cm^{-1} (Fig. 7c, Table 3).

The microscopic images of the FIB films show submicrometer siderite segregations in a siderite matrix (Fig. 8, Table 9), with shapes and sizes varying from place to place (Fig. 8, Table 9). Siderite was identified by TEM, based on EDS microprobe analysis, element mapping (Fig. 8), and EELS. The electron energy loss spectra show bands at 290 and 301 cm^{-1} corresponding to siderite (Garvie and Craven, 1994). The siderite segregations are aggregates of nanocrystals and are often surrounded by rims containing amorphous SiO_2, Ni phosphide crystals of uncertain stoichiometry, and specks of amorphous carbon (Fig. 9b). Isolated Ni phosphide nanocrystals of unknown stoichiometry were also found in association with amorphous SiO_2 and amorphous carbon in larger siderite segregations (Fig. 9b).

Along with siderite segregations, the schreibersite matrix hosts local embayments of gray contrast that

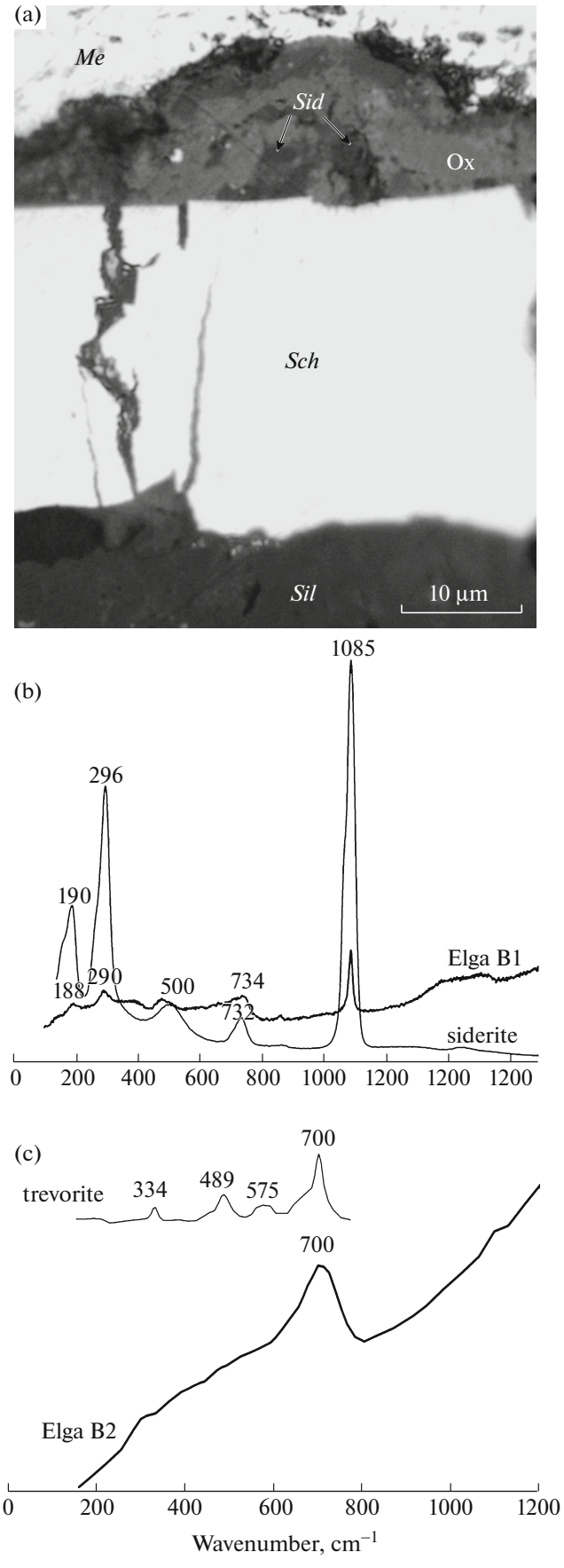

Fig. 5. Siderite in oxide rim on metal (Fig. 1, area *B*). (a) Dark-contrast domains (siderite) in a metal oxidation rim. Phases: *Sid*—siderite, *Ox*—oxide, *Sil*—silicate, *Me*—metal, *Sch*—schreibersite. Optical micrograph taken in reflected light. (b) Raman spectrum of Elga B1, from a dark-contrast part corresponding to siderite. (c) Raman spectrum of Elga B1, from a gray-contrast part corresponding to trevorite (Ahlawat and Sathe, 2011).

form a network of vermicular inclusions (Figs. 9a, 9c). The EDS spectra of these enclaves (Fig. 9d) indicate the presence of oxygen and concentrations of iron and phosphorus that are lower than in schreibersite (Fig. 9e). Obviously, the EDS spectra of the gray contrast areas suggest a superposition of schreibersite underneath and the gray-contrast oxide phase with Fe/Ni ratio lower than in schreibersite. The regions of vermicular microtexture in BSE SEM images may be compared related to pale gray regions in the inclusion in Fig. 7a, whose Raman spectra indicate the presence of trevorite (Fig. 7c). Certain parts of the vermicular trevorite network host rounded black inclusions (Fig. 7b) whose EDS spectra provide evidence of the presence of oxygen, carbon, iron, and silicon.

DISCUSSION

Our study of the fragment 2315-3.3 of the Elga meteorite resulted in identification of carbon-bearing phases: siderite and amorphous carbon. None of these phases have ever been found in any other IIE iron meteorites, and this casts doubt onto the extraterres-

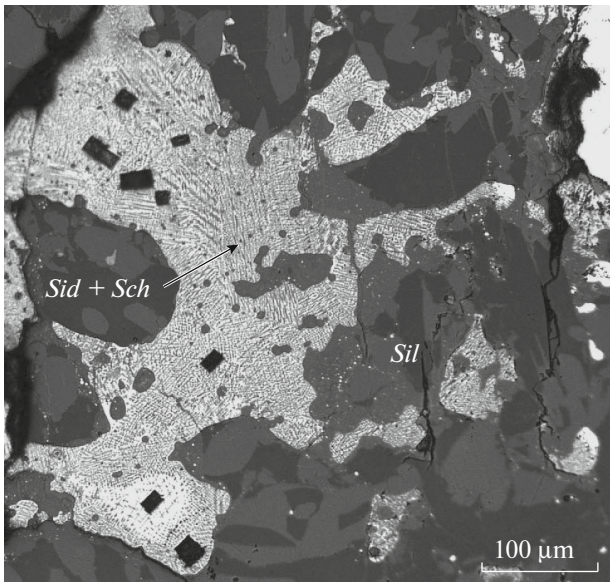

Fig. 6. Schreibersite fragments with a "metal graphic" microtexture in a melting pocket in a silicate inclusion (Fig. 1, area C). Black rectangles in schreibersite are the sites from which the FIB films were cut off. Optical micrograph taken in reflected light.

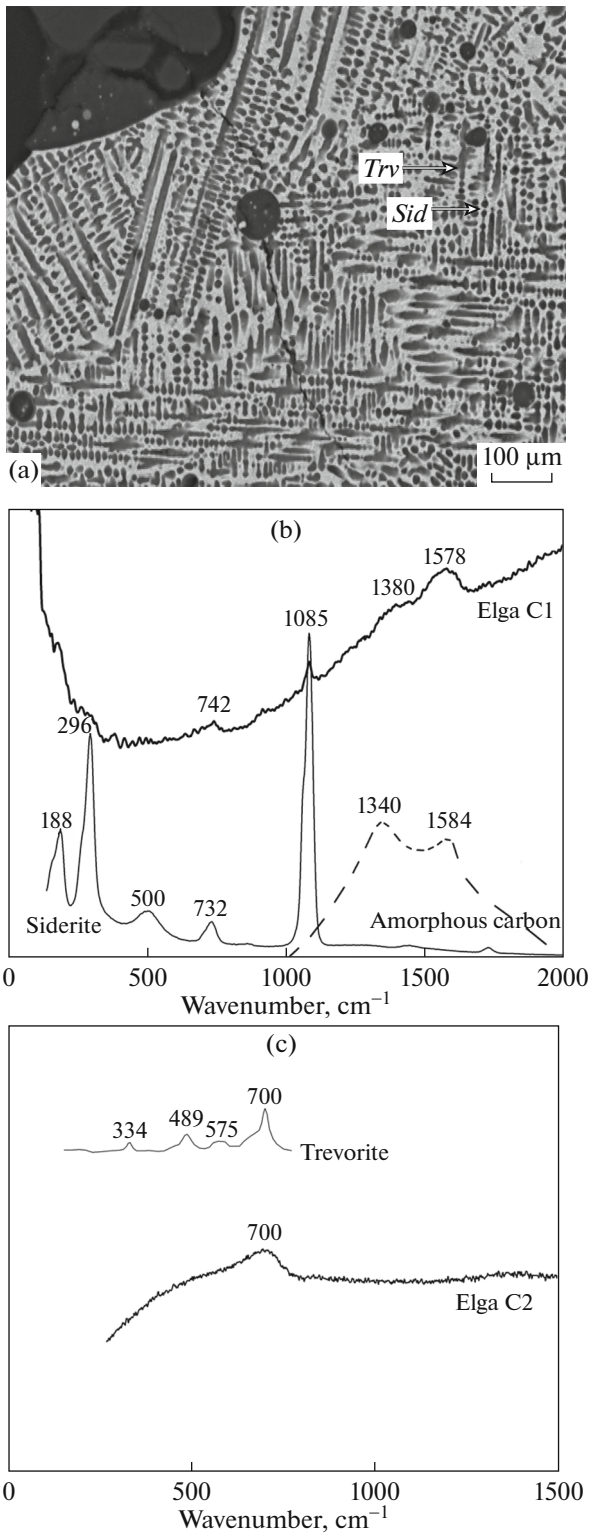

Fig. 7. Siderite, amorphous carbon, and trevorite in a schreibersite fragment with a "metal graphic" microtexture. (a) Enlarged part of the schreibersite fragment shown in Fig. 6. The fragment hosts silicate globules. The "metal graphic" microtexture is defined by a spatially ordered distribution of two phases of darker (siderite) and paler (trevorite) contrast in schreibersite (white). BSE SEM image. (b, c) Raman spectra of the darker segregation (Elga C1 spectrum) and a paler segregation (Elga C2 spectrum). (b) Elga C1 spectrum corresponds to siderite (Buzgar and Apopei, 2009) and amorphous carbon (Larsen and Nielson, 2006); (c) Elga C2 spectrum corresponds to trevorite (Ahlawat and Sathe, 2011).

trial origin of Elga. However, our data on the inner structure of the carbon-bearing fragments and their restricted localization within zones of shock-induced transformations suggest that the occurrence of disordered sp^2 carbon and siderite in the Elga meteorite cannot be explained by terrestrial weathering or contamination of the sample when it was prepared for analysis.

The carbon-bearing phases are typically constrained within the oxide rims that replaced metal at the metal/silicate interface and adjacent schreibersite rims. The double oxide–schreibersite rims at metal–silicate contacts were interpreted as a product of redox reactions between the metal and silicate melt (Osadchii et al., 1981) in the course of the impact process when the meteorite was formed, i.e., when the metallic projectile collided with the silicate target. The fragmentation and brecciation of the rims, the formation of the melt pockets, and the embedding of the brecciated fragments occurred during another (later) impact event. The carbon-bearing phases are found in the oxide rims in association with Ni-magnetite or trevorite $NiFe_2O_4$. Note that the carbon-bearing phases are constrained within a few domains in the meteorite fragment (Fig. 1). The siderite–trevorite association was also found in some rim segments that are not fragmented (Fig. 5). The carbon–oxide fragments are found together with metal and schreibersite fragments in the zone where rims are fragmented in the silicate vein (Fig. 4). Siderite and disordered sp^2 carbon are hosted in oxide–schreibersite fragments of the breccia that were displaced by the impact process into a silicate melt pocket (Fig. 6). Thus, siderite and carbon occur in zones of impact-induced transformations of the material, which were more intense at the metal/silicate interface.

The microtexture, chemistry, and phase heterogeneity of the carbon-bearing schreibersite fragments displaced by the impact process from the silicate–metal boundary into a melt pocket (Figs. 6, 7) suggest the operation of complicated processes of phase and chemical segregation as a consequence of liquid immiscibility of the phosphide–oxide–silicate–carbonate melt. This also follows from the widespread spatial separation of siderite and trevorite in the schreibersite matrix, the morphology of these segregations, the development of the SiO_2 rims around the siderite, and the occurrence of nanocrystals of Ni-bearing phosphide and inclusions of disordered sp^2 carbon in the siderite segregations and in the SiO_2

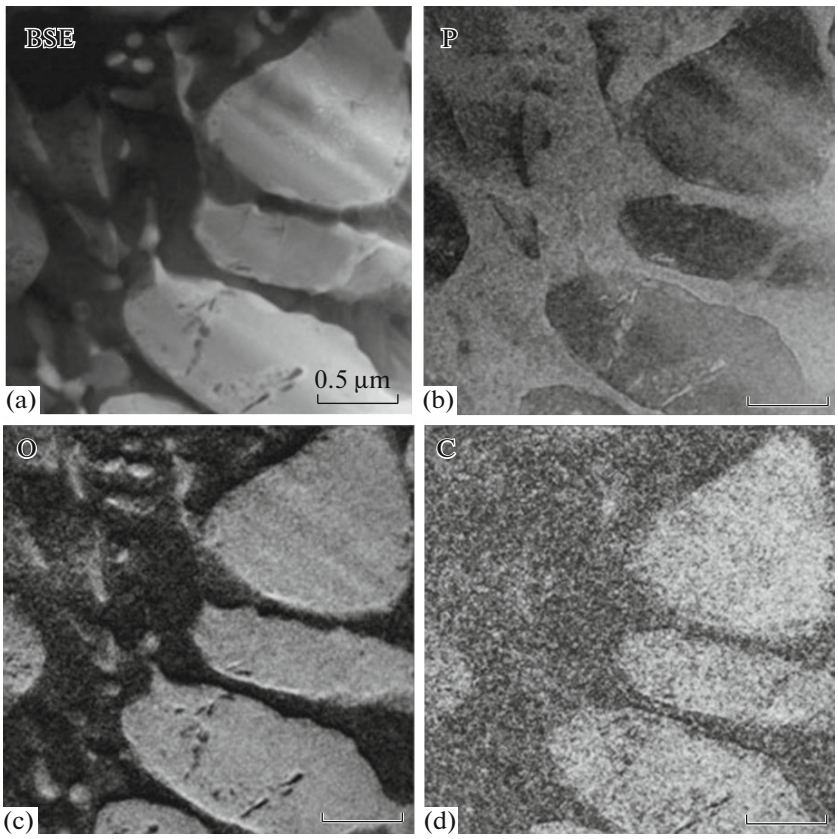

Fig. 8. (a) BSE/TEM image and element mapping of (b) phosphorus, (c) oxygen, and (d) carbon in siderite segregations in a siderite–schreibersite fragment.

rims. The data presented above led us to suggest that the carbon-bearing schreibersite fragments were formed as a result of the impact-induced mixing of compositionally distinct melts, i.e., in the process of "fusing" components of the oxide and schreibersite rims with the carbon and silicate materials. The occurrence of silicate globules in the fragments (Fig. 6) also suggests that these fragments were melted during relatively brief time spans. Numerous silicate globules in the schreibersite and schreibersite globules in the silicate glass (Fig. 3) resulted from silicate–phosphide liquid immiscibility in the impact melt of the melt pocket.

Our data suggest an extraterrestrial origin of the disordered sp^2 carbon and siderite in the Elga meteorite and allowed us to compare them with carbon-bearing phases in other meteorites.

Carbon is widespread in space. Amorphous carbon was found in the matrix of carbonaceous chondrites, various carbon species were identified in the Allende (Smith and Busek, 1981) and ALH 84001 Martian meteorite (Steele et al., 2007, 2012). The Raman spectra of carbon inclusions in the oxidation rim of FeNi metal in Elga (Fig. 4) are similar to the spectra of amorphous carbon in the Murchison carbonaceous chondrite (King et al., 2011) and to the spectra of macromolecular (or amorphous) carbon in the Martian meteorite (Steele et al., 2012). It is pertinent to recall that carbon-forming processes in carbonaceous chondrites and Martian meteorites are principally different. In carbonaceous chondrites, carbon is formed via thermal transformations of organic matter. As known, solid carbon is formed from organic matter at high temperatures and pressures. For example, polycrystalline graphite was synthesized by impact heating under a pressure of about 30 GPa in experiments on impact-induced transformations of bitumen as analogues of meteoritic organic matter (Korochantsev, 2007). Carbon occurs in ALH 84001 in association with magnetite, which envelops siderite granules 50–250 μm in diameter (Steele et al., 2007, 2012). Currently available extensive experimental data make it possible to rule out an organic origin of siderite globules in Martian meteorites and suggest a hypothesis of siderite decarbonatization as a mechanism able to produce the magnetite–carbon association in ALH 84001(Bell, 2007).

Siderite is very seldom found in meteoritic material and is thought to be a secondary mineral of extraterrestrial nature. This mineral was found in Martian meteorites (Hicks et al., 2014; Bridges and Grady, 2000; Golden et al., 2001; and others) and in carbonaceous chondrites (Weisberg et al., 1993; Tyra et al., 2010; Lindgren et al., 2013; Leuw et al., 2010; and oth-

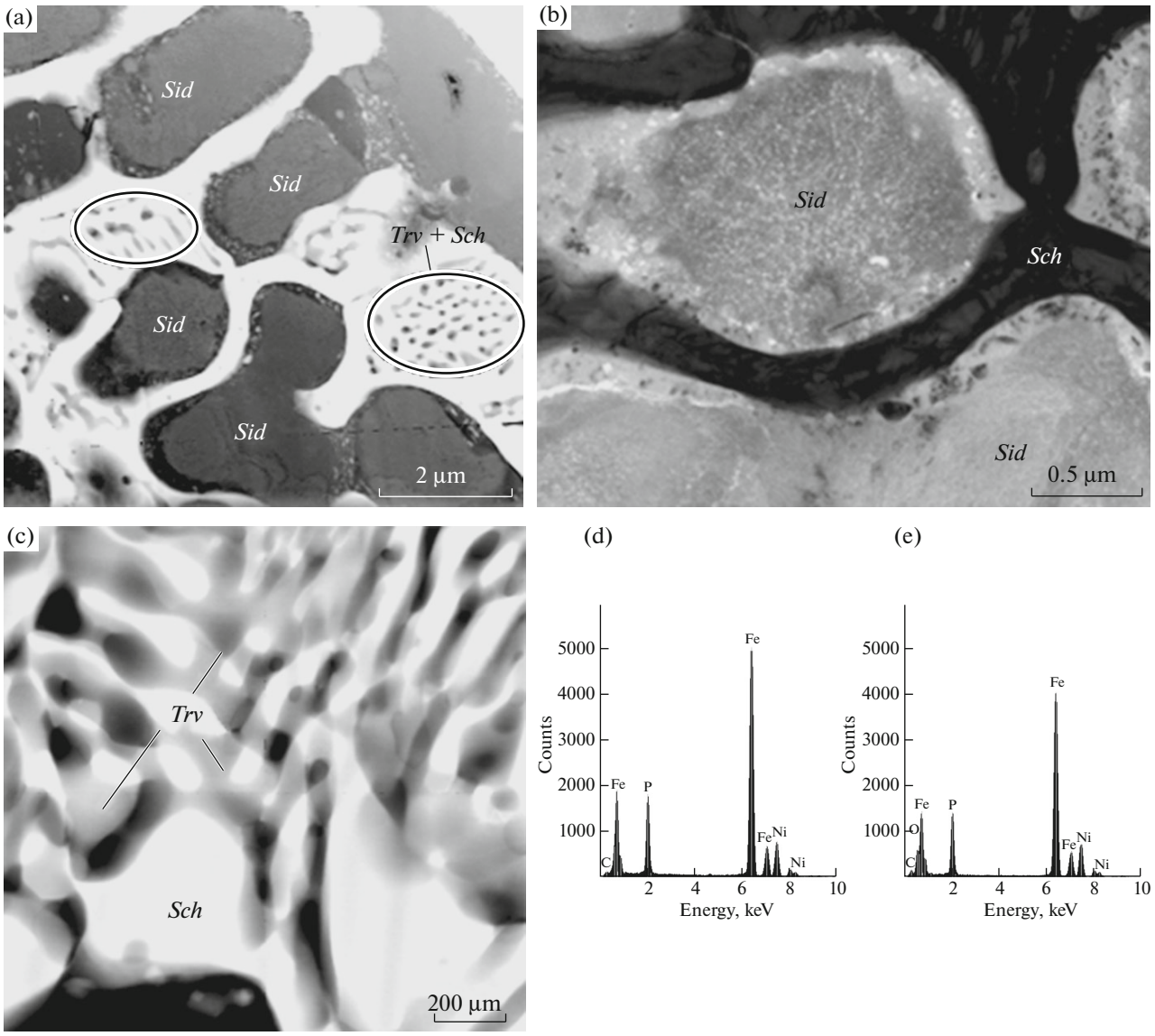

Fig. 9. TEM image of a multiphase fragment. (a) Part of the schreibersite fragment with large siderite (*Sid*) segregations and areas with vermicular trevorite (*Trv*) segregations in schreibersite matrix (white). Ovals mark trevorite segregations. (b) SiO_2 rims (pale) around siderite and disseminated amorphous carbon (white specks) and Ni phosphide of unknown stoichiometry (black specks) in siderite in the rims. TEM, bright-field image. (c) Enlarged image of the material hosting trevorite (*Trv*) shown in Fig. 9b and (d) the corresponding EDS spectra of the schreibersite matrix and (e) trevorite–schreibersite aggregates.

ers). Siderite was identified in the Nakhla, Lafayette, and Valadares nakhlites (Hicks et al., 2014; Bridges and Grady, 2000; and others) and in the ALH 84001 meteorite (Gleason et al., 1997; Golden et al., 2001; Steele et al., 2007, 2012; and others). In nakhlite, siderite lines the walls of cracks in olivine or between olivine and pyroxene and was also identified in veinlets, usually in association with silicate gel and sometimes also with phyllosilicates. In the ALH 84001 Martian meteorite, siderite in association with magnetite was found in the form of patchy segregations up to 100 μm across, single crystals, and globules in fractured zones of the orthopyroxene rock (Thomas-Kerpta et al., 2009; Gleason et al., 1997). Currently most researchers are prone to believe that siderite in Martian meteorites is most probably of extraterrestrial inorganic origin. Arguments that siderite in nakhlites could be formed by hydrothermal brines (CO_2-bearing fluids) are presented in (Hicks et al., 2014). Gleason et al. (1997) thought that siderite in ALH 84001 is a secondary carbonate of extraterrestrial origin, which was likely formed by dissolution and replacement reactions between CO_2-bearing fluid and feldspathic glass of the meteorite in a Martian environment. Scott et al. (1997) suggested a model for the origin of the siderite globules in ALH 84001 as a consequence of

impact melting. In the context of an extraterrestrial origin of the siderite, it is also pertinent to mention the amazing find of siderite in association with the oxihydroxide FeOOH in impact breccia 65903, 16-7 from the Apollo 16 lunar collection (Zeigler et al., 2001). The siderite was interpreted as resulting from the carbonatization process that took place on the Moon under the effect of fluid generated by the evaporation of the projectile rich in volatiles.

CONCLUSIONS

Our EMPA, TEM, and Raman spectroscopic data indicate that the Elga meteorite hosts carbon-bearing phases: siderite and amorphous sp^2 carbon, none of which have ever been found in IIE iron meteorites. Comparison of the carbon-bearing phases in Elga and in carbonaceous chondrites and Martian meteorites led us to look for their differences. In contrast to Martian meteorites, amorphous sp^2 carbon and siderite in Elga are hosted not in the silicate material but in an oxide rim on the metal. This explains the reasons for the compositional differences of siderite in Elga and Martian meteorites, with the latter hosting siderite rich in Ca and Mn. The most important difference of siderite in Elga and Martian meteorites and carbonaceous chondrites is that carbon-bearing phases in Elga are obviously constrained within impact brecciation and melting zones at boundaries between the metal and silicate and that these phases occur in association with fragments of the oxide rims replacing the metal. Our results led us to conclude that carbon-bearing phases in the Elga meteorite are of extraterrestrial origin and were produced in relation to shock metamorphism. An organic or inorganic source of carbon in Elga and the reactions that could form the sp^2 carbon and siderite in the impact process require further studies.

ACKNOWLEDGMENTS

The authors thank D.D. Badyukov, E.G. Osadchii, A.A. Kadik, and K. Litasov for valuable consultations and discussion of materials presented in the manuscript. We appreciate comments on the manuscript provided by A.A. Ul'yanov and the anonymous reviewer. The Raman spectroscopic measurements were carried out at the CKP FMI at the Frumkin Institute of Physical Chemistry and Electrochemistry, Russian Academy of Sciences. This study was partly financially supported under Program 7 of the Presidium of the Russian Academy of Sciences and the Russian Foundation for Basic Research, project no. 15-05-03351.

REFERENCES

A. Ahlawat and V. G. Sathe, "Raman study of $NiFe_2O_4$ nanoparticles, bulk and films: effect of laser power," J. Raman Spectrosc. **42**, 1087–1094 (2011).

P. Beck, T. Ferroir, and P. Gillet, "Shock-induced compaction, melting and entrapment of atmospheric gases in Martian meteorites," Geophys. Res. Lett. **34**, L01203 (2007).

M. S. Bell, "Experimental shock decomposition of siderite and the origin of magnetite in martian meteorite ALH 84001," Meteorit. Planet. Sci. **42** (6), 935–949 (2007).

J. C. Bridge and M. M. Grady, "Evaporite mineral assemblages in the nakhlite (Martian) meteorites," Earth Planet. Sci. Lett. **176**, 267–279 (2000).

N. Buzgar, and A. I. Apopei, "The Raman study of certain carbonates," Analele Stiintifice Ale Universitatii, Al. I. Cuza Iasi Geologie **55**, 97–112 (2009).

L. Casanova, T. Graf, and K. Marti, "Discovery of an unmelted H-chondrite inclusion in an iron meteorite," Science **268**, 540–542 (1995).

R. N. Clayton, T. K. Mayeda, E. Olsen, and M. Prinz, "Oxygen isotope relationships in iron meteorites," Earth Planet. Sci. Lett. **65**, 229-232 (1983).

M. I. D'yakonov, V. Ya. Kharitonova, and A. A. Anvel, *Chemical Composition of Meteorites* (Nauka, Moscow, 1979) [in Russian].

M. J. Gaffey and S. L. Gilbert, "Asteroid 6 Hebe: the probable parent body of the H-type ordinary chondrites and the IIE iron meteorites," Meteorit. Planet. Sci. **33**, 1281–1295 (1998).

L. A. J. Garvie and A. J. Craven, "Use of electron-energy loss near-edge structure in the study of minerals," Am. Mineral. **79**, 411–425 (1994).

J. G. Gleason, D. A. Kring, D. H. Hill, and W. V. Boynton, "Petrography and bulk chemistry of Martian orthopyroxenite ALH 84001: implications for the origin of secondary carbonates," Geochim. Cosmochim. Acta **61**, 3503–3512 (1977).

D. C. Golden, D. W. Ming, C. S. Schwandt, H. V. Lauer, Jr., R. A. Socki, R. V. Morris, G. E. Lofgren, and C. A. McKey, "A simple inorganic process for formation of carbonates, magnetite, and sulfides in Martian meteorite ALH 840001," Am. Mineral. **86**, 370–375 (2001).

P. R. Graves, C. Johnston, and J. J. Campaniello, "Raman scattering in spinel structure ferrites," Mater. Res. Bull. **23**, 1651–1660 (1988).

L. J. Hicks, J. C. Bridges, and S. J. Gurman, "Ferric saponite in the nakhlite martian meteorites," Geochim. Cosmochim. Acta **136**, 194–210 (2014).

Y. Ikeda and M. Prinz, "Petrology of silicate inclusions in the Miles IIE iron," Proc. NIPR Symp. Antarct. Meteorites **9**, 143–173 (1996).

N. R. Khisina, A. A. Shiryaev, A. A. Averin, S. V. Teplyakova, and R. Wirth, "Raman spectroscopy of carbonaceous and oxide phases in impact melted zones of Elga meteorite," GeoRaman-2016, abstract # 67 (2016).

A. King, T. Henkel, S. Chapman, H. Busemann, D. Rost, C. Guillermier, M. R. Lee, I. A. Franchi, and I. C. Lion, Amorphous carbon grains in the Murchison meteorite," Lunar Planet. Sci. Conf. **42**, #2604 pdf (2011).

A. V. Korochantsev, PhD Thesis (GEOKhI, Moscow, 2007) [in Russian].

G. Kurat, M. E. Varela, and E. Zinner, "Silicate inclusions in the Kodaikanal IIE iron meteorite," Lunar Planet. Sci. Conf. **36**. #1814 pdf (2005).

G. Kurat, E. Zinner, and M. E. Varela, "Trace element studies of silicate-rich inclusions in the Guin (UNGR) and Kodaikanal (IIE) iron meteorites," Meteorit. Planet. Sci. **42**, 1441–1463 (2007).

L. G. Kvazha, Yu. G. Lavrent'ev, and N. V. Sobolev, "Silicate inclusions and evidence of impact metamorphism in the Elga octahedrite," Meteoritika **33**, 143–147 (1974).

K. L. Larsen and O. F. Nielsen, "Micro-Raman spectorscopic investigations on the carbonaceous meteorites Allende, Axtell and Murchison, J. Raman Spectrosc. **37**, 217–222 (2006).

S. A. Leuw, E. Rubin, and J. T. Wasson, "Carbonates in CM chondrites: complex formation histories and comparison to carbonates in CI chondrites," Meteorit. Planet. Sci. **45** (4), 513–530 (2010).

P. Lindgren, M. R. Lee, M. R. Sofe, and M. E. Zolensky, "Clasts in the CM2 carbonaceous chondrite Lonewolf Nunataks 94101: evidence for aqueous alteration prior to complex mixing," Meteorit. Planet. Sci. **48** (6), 1074–1090 (2013).

T. J. McCoy, "Silicate-bearing IIE irons: early mixing and differentiation in a core-mantle environment and shock resetting of ages," Meteoritics **30**, 542–543 (1995).

K. H. McDermott, R. C. Greenwood, I. A. Franchi, M. Anand, and E. R. D. Scott, "The formation of the IIE iron meteorites," Lunar Planet. Sci. Conf. **45** #1910 pdf (2014).

E. Olsen, A. Davis, R. J. Clarke, Jr., L. Schultz, and H. W. Weber, "Watson: A new link in the IIE iron chain," Meteoritics **29**, 200–213 (1994).

E. G. Osadchii, G. V. Baryshnikova, and G. V. Novikov, "The Elga meteorite: Silicate inclusion and shock metamorphism," Lunar Planet Sci. **12**, 1049–1068 (1981).

L. N. Plyashkevich, "Some data in composition and structure of the Elga iron meteorite," Meteoritika **22,** 51–60 (1962).

G. Rana and U. C. Johri, "A study on structural and magnetic properties of Ni-substituted magnetite nanoparticles,' J. Alloys Compounds **577**, 376–381 (2013).

E. R. D. Scott A. N. Krot, and A. Yamaguchi, "Formation of carbonates in martian meteorite ALH84001 from schock melts," Meteorit. Planet. Sci. **32**, A117 (1997).

P. P. K. Smith and P. R. Buseck, "Graphitic carbon in the Allende meteorite: a microstructural study," Science **212**, 322–324 (1981).

A. Steele, F. M. McCubbin, M. D. Fries, D. C. Golden, D. Ming, and L. G. Benning, Graphite in the martian meteorite Allan Hills 84001," Am. Mineral. **97**, 1256–1259 (2012).

A. Steele, M. D. Fries, H. E. F. Amundsen, B. O. Mysen, M. L. Fogel, M. Schweizer, and N. Z. Boctor, "Comprehensive imaging and Raman spectroscopy of carbonate globules from martian meteorite ALH 84001 and a terrestrial analogue from Svalbard," Meteorit. Planet. Sci. **42**, 1549–1566 (2007).

S. N. Teplyakova, M. Humayun, C. A. Lorenz, and M. A. Ivanova, "A common parent for IIE iron meteorites and H chondrites, *Lunar Planet. Sci. Conf.* **43**, abstract #1130.pdf (2012).

S. N. Teplyakova, "Evolution of molten material in iron cores of small planets," Solar Syst. Res., **45** (6), 515–522 (2011).

S. N. Teplyakova, N. R. Khisina, V. V. Artemov, and A. L. Vasil'ev, "Nanomineralogy of dendritic inclusions in the Elga iron meteorite," Zap. Ross. Mineral. O-va, **141** (2), 42–52(2012).

S. N. Teplyakova, Yu. A. Kostitsyn, and N. N. Kononkova, "Differentiated precursor for silicate inclusions in the Elga iron meteorite," *Lunar Planet. Sci. Conf.* **41,** abstract #1686 (2010).

K. L. Thomas-Kerpta, S. I. Clemett, D. S. McKay, E. K. Gibsen, and S. J. Wentworth, "Origin of magnetite nanocrystals in martian meteorite ALH84001," Geochim. Cosmochim. Acta **73**, 6631–6677 (2009).

M. A. Tyra, J. Matzel, A. J. Brearley, I. D. Hutcheon, "Variability in carbonate petrography and nanosims $^{53}Mn/^{53}Cr$ systematic in paired CM1 chondrites ALH 84049 and ALH 84034," *Lunar Planet Sci.* **41**, #2687 pdf (2010).

F. Ulff-Møller, K. L. Rusmussen, M. Prinz, H. Palm, and B. Spettel, "Magmatic activity on the IVA parent body: Evidence from silicate-bearing iron meteorites," *Geochim. Cosmochim. Acta* **59**, 4713–4728 (1995).

V. I. Vronskii, "On the find of the Elga iron meteorite," Meteoritika **22**, 47–50 (1962).

J. T. Wasson, "Ni, Ga, Ge and Ir in the metal of iron meteorites with silicate inclusions," Geochim. Cosmochim. Acta **34**, 957–964 (1970).

M. K. Weisberg, M. Prinz, R. N. Clayton, and T. K. Mayeda, "The CR (Renazzo-type) carbonaceous chondrite group and its implications," Geochim. Cosmochim. Acta **57**, 1567–1586 (1993).

B. L. Zeigler, A. Jolliff, R. L. Wang, D. T. Korotev, D. T. Kremser, and L. A. Haskin, "Formation of carbonate and oxyhydroxide minerals by impact of a volatile-rich body," Lunar Planet. Sci. Conf. **32**, abstract #1243 pdf (2001).